ATMOSPHERIC SCIENCE LETTERS
Atmos. Sci. Let. **10**: 48–57 (2009)
Published online 23 January 2009 in Wiley InterScience
(www.interscience.wiley.com) **DOI:** 10.1002/asl.209

RMetS
Royal Meteorological Society

An integrated analysis of lidar observations in association with optical properties of aerosols from a high altitude location in central Himalayas

P. Hegde,[1†*] P. Pant[1] and Y. Bhavani Kumar[2]
[1]*Aryabhatta Research Institute of Observational Sciences (ARIES), Nainital, India*
[2]*National Atmospheric Research Laboratory (NARL), Gadanki, India*

**Correspondence to:*
P. Hegde, Aryabhatta Research Institute of Observational Sciences (ARIES), Nainital, India.
E-mail: hegdeprashant@yahoo.com

[†]*Current address: Space Physics Laboratory (SPL), Vikram Sarabhai Space Centre (VSSC), Indian Space Research Organization, Trivandrum-695022 Kerala, India.*

Received: 4 April 2008
Revised: 21 November 2008
Accepted: 3 December 2008

Abstract

In order to study the aerosol backscatter profiles, a portable micro pulse lidar (MPL) system was installed in the year 2006 at Manora Peak, (29°22′N, 79°27′E, ∼1960 m amsl) Nainital, a high altitude location in the central Himalayas. In the present study the results of observed lidar profiles, columnar aerosol optical depths (AOD) and prevailing meteorology during May 2006 to June 2007 are presented. Although the lidar was operated from a sparsely inhabited free tropospheric site, nevertheless the height distribution of aerosol layers are found to be extended up to the summit of ∼2 km above the ground level (AGL). The backscatter ratio (BSR) varies from ∼10 to ∼20 having lowest values during post-monsoon and highest during pre-monsoon period. The observed boundary layer height during the post monsoon was shallower to the pre-monsoon period. Occasionally the lidar profiles reveal the presence of cirrus clouds at an altitude of 8–10 km AGL. The extended lidar observations over Manora Peak not only provided the profiles of aerosol extinction coefficient but also significantly substantiate the elevated aerosol layers and clouds, which are important in the study of climate modelling. Copyright © 2009 Royal Meteorological Society

Keywords: **lidar profiles; atmospheric aerosols; backscatter ratio; cirrus clouds**

1. Introduction

Atmospheric aerosols have a direct effect on the radiative forcing in the atmosphere as they scatter and absorb solar and infrared radiation in the atmosphere (Charlson *et al*., 1992) and indirectly affect the size distribution of cloud droplets (IPCC, 2007). It is an established fact that aerosols significantly affect the earth radiation budget through the scattering and absorption of incoming solar radiation. In this perspective the temporal and spatial distributions of aerosol in the lower atmosphere are important in assessing their impact on the earth's climate. In addition to these effects, aerosols also play an important role in providing the information on the development of cloud microphysics, climate variability, atmospheric pollution and atmospheric boundary layer evaluation (Lagrosas *et al*., 2004). Lidar has so far shown the best performance in defining the position of aerosol and clouds with high temporal and spatial resolution, which is not possible with other kind of remote sensing techniques (Devara *et al*., 1995; Raj *et al*., 1996). Lidar can provide vertically resolved extinction and backscatter coefficients, and thereby providing the height of the planetary boundary layer or the night-time residual layer. A thorough knowledge of optical properties of atmospheric aerosol such as the extinction and optical depth as well as their temporal and vertical distribution are essential for understanding their effects on the atmosphere.

Lidar has also proven to be a powerful means to study cloud characteristics particularly of cirrus clouds with high range and time resolution. These clouds are usually found at an altitude, ranging from 8 to 20 km Devara *et al*., 1995; and often extend to more than 1000 km horizontally and persist for up to several days (Immler and Schrems, 2002). These clouds are produced by the outflow of deep convection cloud anvils of the slow synoptic scale uplifting of a moist air layer and homogeneous nucleation (Thomas *et al*., 2002). Although the role of the tropical cirrus clouds in the overall global climate system is not completely understood however they dominate the cloud radiative forcing especially over the tropics (Sunil Kumar *et al*., 2003). Parameswaran *et al*. (1991) compared the aerosol extinction profiles derived from Sage II satellite data with lidar observations over tropical coastal station, Trivandrum (Figure 1). They found large day to day as well as latitudinal and longitudinal changes in tropospheric extinction, which points out the importance of the study of tropospheric aerosol extinction at different locations even within the tropical region for understanding of the behaviour of tropospheric aerosols.

Over the years, several ground and space based lidar observations were simultaneously conducted over the East Asian region (e.g. Murayama *et al*., 2003,

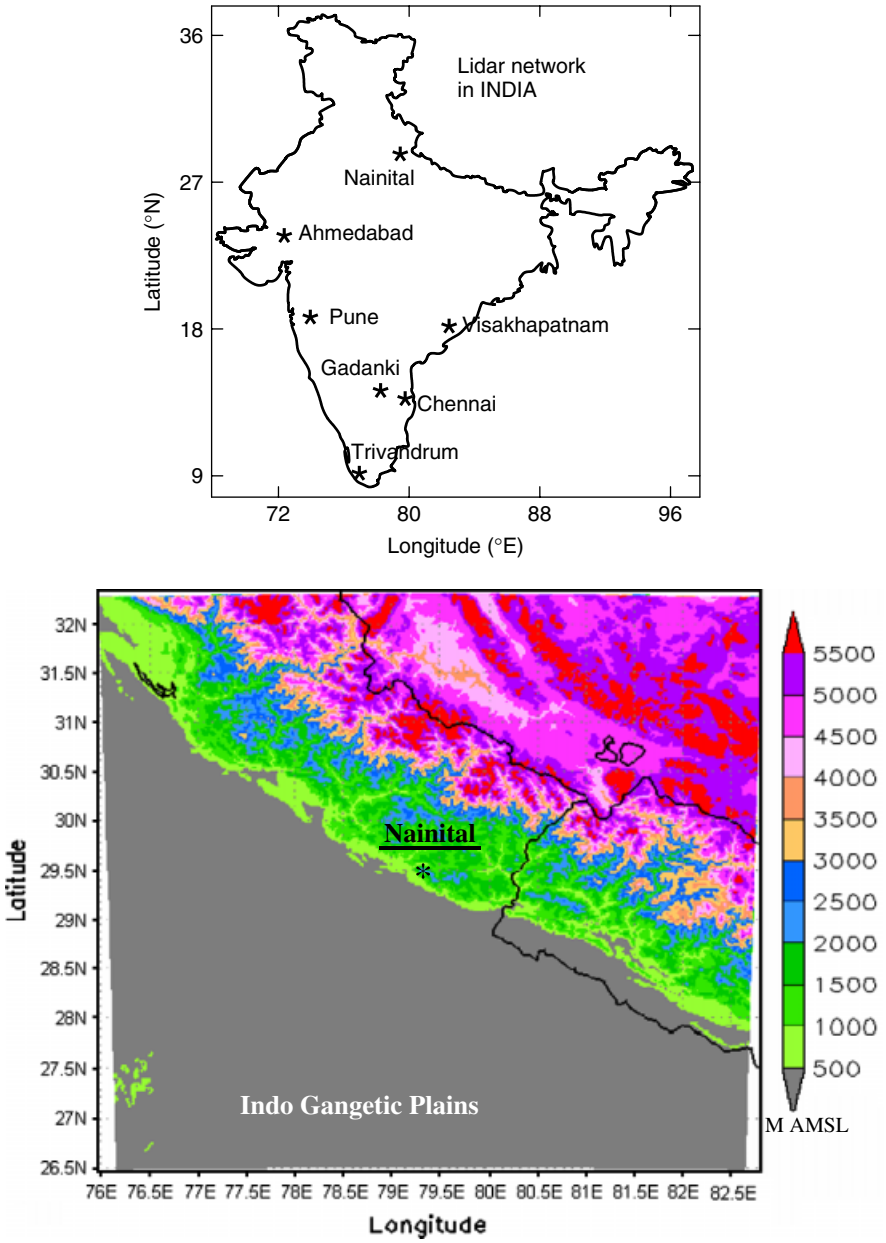

Figure 1. List of lidar network stations in India (upper panel), topography map of west central Himalayan region adjacent to Indo Gangetic Plains (lower panel).

and references therein) during an integrated campaign under aerosol characterisation experiment (ACE), but such observations are sparse over Indian subcontinent. In this perspective seven lidar network stations have recently been established (Figure 1).

As a part of this network, a portable micro pulse lidar system was installed at ARIES, Manora Peak, Nainital (29°22′N, 79°27′E, elevation – 1960 m amsl), a high altitude location in central Himalayas (Figure 1) for the study of aerosol backscatter profiles and clouds. The north and northeast of Manora Peak has sharply undulating topography of Himalayan mountain ranges, where as very low elevation and densely populated plain land merging in to the Ganga basin to the southwest (Pant *et al*., 2006). Owing to its large elevation, this site is considered to be a free tropospheric site. As the site is located geographically in free troposphere and is reasonably sparse from the point of view of major pollution, the investigation from such a remote, sparsely inhabited regions have the importance of providing a sort of background level against which the aerosol loading impact in the atmosphere can be assessed.

2. Instrumentation and methodology

The portable micro pulse lidar for atmospheric aerosol studies has been installed in a temperature and humidity controlled room. The lidar system is designed and developed by National Atmospheric Research Laboratory (NARL) Gadanki (Bhavani Kumar, 2006) which is based on micro pulsed lidar (MPL) technology (Spinhirne, 1993; Cambell *et al*., 2003; Cheng *et al*.,

DOI: 10.1002/asl

2005). Lidar observations are carried out at Nainital on regular basis to study the aerosol vertical profile, the boundary layer structures, cloud base height and its vertical extent. The system employs a diode pumped Nd : YAG laser with second harmonic output at 532 nm and operated at 2500 Hz. The emitter beam is coaxial to receiver field of view (FOV) and operated in zenith direction. The lidar receiver employs a 150-mm cassegrainin telescope and a high gain photo multiplier tube (PMT) operating in photon counting mode. The complete overlap between the laser beam and the telescope FOV is expected at ~150 m. This value represents the lower limit of our vertical lidar profiles. The backscattered signals are measured with a bin width of 200 ns corresponding to the altitude range of 30 m. Computer based multichannel analyser (MCA) was employed for recording the photon returns. During the observations the lidar system collects the backscattered signal returns from the lower atmospheric aerosol and high altitude cloud such as cirrus. The data were processed using algorithm described by Fernald (1984) and Klett (1985) for deriving the aerosol extinction coefficient profiles and other related atmospheric parameters. The inversion lidar profiles are based on the solution of the lidar equation for the case of single scattering (Measures, 1984), given as:

$$P(\lambda, R) = P_L A_O \frac{\xi(\lambda)}{R^2} \beta(\lambda, R) \zeta(R) \frac{c\tau_1}{2} \exp\left[-2\int_0^R \alpha(\lambda, R) dR\right] \quad (1)$$

where, $P(\lambda, R)$ is the lidar signal received from a range R at a wavelength λ, P_{L} is the emitted laser power, A_{o} is the telescope receiving area, $\xi(\lambda)$ is the receivers spectral transmission factor, $\beta(\lambda,\mathrm{R})$ is the atmospheric volume backscattering coefficient, $\zeta(\mathrm{R})$ is the overlap factor between the FOV of the telescope and the laser beam, $\alpha(\lambda,\mathrm{R})$ is the extinction coefficient from atmospheric molecules and particles, c is the speed of light and τ_{l} is the laser pulse length. The lidar data have been processed with the algorithm described by (Fernald, 1984; Klett, 1985), where the molecular (or Rayleigh) contribution to the signal is taken from the COSPAR International Reference Atmosphere (CIRA) 1986 standard atmosphere. According to the Fernald–Klett formulation, the solution of the lidar equation is given as:

$$\beta(R) = \frac{\exp\{-[S'(R_{\mathrm{ref}}) - S'(R)]\}}{\frac{1}{\beta(R_{\mathrm{ref}})} + \frac{2}{C}\int_R^{R_{\mathrm{ref}}} dR' \exp\{-[S'(R_{\mathrm{ref}}) - S'(R')]\}} \quad (2)$$

where, the total backscattering coefficient is the sum of Rayleigh and particulate contribution given by $\beta(\mathrm{R}) = \beta_{\mathrm{p}}(\mathrm{R}) + \beta_{\mathrm{R}}(\mathrm{R})$, the $\beta(\mathrm{R_{ref}})$ is the boundary condition set on β(R) at the reference far-end range. The solution to the above equation is given numerically as under:

$$S'(R_{\mathrm{ref}}) - S'(R) = \ln[R_{\mathrm{ref}}^2 \times P(R_{\mathrm{ref}})] - \ln[R^2 \times P(R)] - \frac{3}{4\pi}\int_R^{R_{\mathrm{ref}}} \beta_R(R') dR' + \frac{2}{C}\int_R^{R_{\mathrm{ref}}} \beta_R(R') dR' \quad (3)$$

The above equations were derived by taking the value of C equal to 0.035, an average value for rural, urban and maritime aerosols (Kovalev, 1993), the reference range (R_{ref}) in a region where the lidar profile follows the molecular atmosphere (generally between 4 and 6 km) and assuming that the backscatter-to-extinction ratio is known. Besides the lidar observations the measurements of aerosol optical depth using the Microtops II, Sun Photometer (Solar Light Co., USA) and meteorological parameters using, standard meteorological sensors (Campbell Scientific Inc., Canada) attached with automatic weather stations, were also carried out.

3. Results and discussion

3.1. Surface meteorology

The monthly mean variations of surface meteorological parameters for temperature, columnar water vapour, rainfall, wind speed and wind direction at Manora Peak are provided in Table I. Monthly mean temperature varies from its maximum value of 28.5 °C during May and shows gradual decreasing trend during rainy season and minimum temperatures occur during January and February. The columnar water vapour content remains less than 1 cm in 80% of the measurements, with a mean value of 0.64 cm implying a dry environment. Humidity is particularly high with the arrival of monsoon from mid June to end of September. The rainfall climatology shows that the rainfall is highest during July to September owing to the southwest monsoon over the Indian subcontinent (accounting ~70% of the annual rainfall), with very little rain during March to middle of June (~10% of the annual). The wind speed, during post-monsoon (September, October and November) and winter months (December, January and February) remains ~10 m s^{-1} but during pre-monsoon (March, April and May) as well as during the monsoon (June, July and August) it is maximum and sometimes reaches up to ~24 m s^{-1}. During the transition period from pre-monsoon to monsoon the mean arrival wind direction gradually shifts from southwesterly to southeasterly.

3.2. Overview of BSR characteristics

For the present study the lidar measurements are analysed for the period of May 2006 to June 2007. The

DOI: 10.1002/asl

Table I. Lidar observation details along with surface meteorology and other parameters (brief description of parameters are included)

Parameters	May	Jun	Jul	Aug	Sep	Oct	Nov	Dec	Jan	Feb	Mar	Apr	May	Jun
	2006								2007					
Profiles	295 (3)	627 (6)	—	—	279 (4)	2098 (13)	1254 (15)	637 (6)	793 (9)	593 (3)	1041 (8)	887 (9)	602 (8)	42 (2)
T_{max}	28.5	28	26	25	25	24	23	21	20	18	22	25	28.5	28
CWV	0.55	0.77	1.83	1.39	1.28	0.63	0.51	0.26	0.24	0.32	0.51	0.48	0.56	0.81
Rainfall	90	120	477	554	253	32	1.3	12	2.4	161	98	29	298	351
WS	23	21	16.4	11.8	9.3	9.4	8.5	8.2	8.8	12	14	13	20.3	17
WD	238	210	150	148	162	222	209	226	236	220	209	251	230	209
Lidar AOD	0.143	0.264	—	—	0.071	0.044	0.041	0.023	0.034	0.042	0.065	0.135	0.176	0.147
M Tops AOD	0.210	0.314	0.082	0.135	0.090	0.062	0.066	0.036	0.050	0.076	0.072	0.163	0.228	0.317
Trajectories	47	38	26	12	10.5	13	10	6	2	4	14	22	34	38
Aerosol index	2.97	1.81	0.68	0.49	0.61	0.72	0.49	−0.37	0.01	0.42	1.35	2.12	2.68	1.63

Profiles, total number of lidar observation profiles each having 2 min duration, below is the number in parentheses give total nights for which observations were made.
T_{max}, maximum temperature (°C).
CWV, columnar water vapour content (cm) derived from Microtops II sunphotometer.
Rainfall, cumulative rainfall (mm).
WS, average wind speed (m/s).
WD, wind direction (Degrees).
Lidar AOD, lidar derived aerosol optical depth (532 nm).
M Tops AOD, microtops II sunphotometer derived aerosol optical depth (500 nm).
Trajectories, percentage of air mass arriving from southwest direction.
Aerosol index, Total Ozone Mapping Spectrometer (TOMS)/Ozone Monitoring Instrument (OMI) satellite aerosol index.

DOI: 10.1002/asl

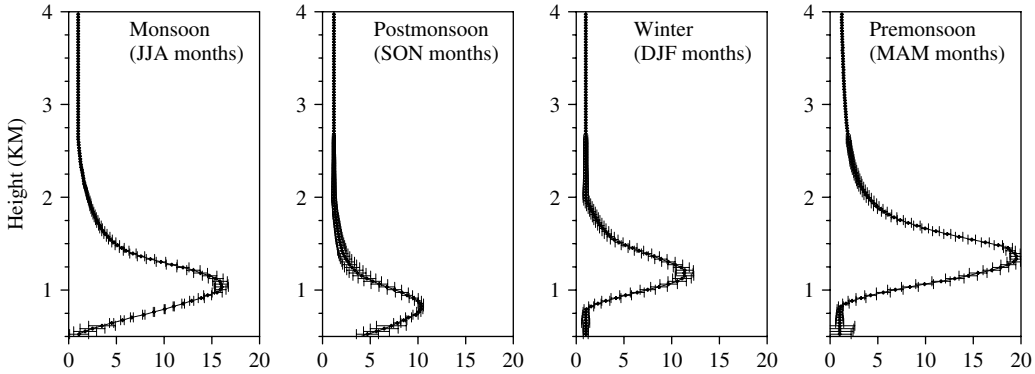

Figure 2. Vertical profiles of back scatter ratio (*R*) averaged for different seasons during May 2006 to June 2007. The horizontal bars represent the one standard deviation.

details of lidar observations along with other parameters are listed in Table I. Generally observations were made from 1900 Indian Standard Time (IST) to 2400 IST, but on few occasions the data were recorded for entire night (i.e. from 1900 IST to 0500 IST). Figure 2 shows the profiles of back scattered ratio (BSR), calculated from the selected profiles representing different seasons. Higher values of BSR are found for the prevailing strong convection conditions during summer months (March, April and May (MAM); when the wind is predominantly from southwesterly. It is quite discernible from the figure that aerosol layer often reaches up to an altitude of ~2.0 km. The lower value of BSR during post-monsoon season [September, October, November (SON)] may be due to rain scavenging of aerosol from the lower troposphere. During summer months (pre-monsoon) the vertical extent of aerosols in the troposphere is large over northwestern part of India due to increase in temperature as well as dust transport from Thar Desert region (Hegde *et al*., 2007). The higher values of BSR over study region are attributed to the strong convective conditions during these months, when aerosol and dust particles are often lifted up to free troposphere over the Northwestern India (Prasad *et al*., 2007). The exchange of air masses from the boundary layer in to the free troposphere is aided by mountain ranges and may thus affect the spatial as well as temporal distribution of aerosol properties (Nyeki *et al*., 2000).

3.3. Mixed layer depth determination

The atmospheric boundary layer can be divided in to three different layers: the surface layer, the mixed layer and the entrainment zone (Stull, 1997). The atmospheric entrainment zone is considered as a thin, convoluted sub-layer that separates the air transported upwards from the mixed layer and the air transported from the free atmosphere aloft (Mok and Rudowicz, 2004). In aerosol studies, the mixed layer characteristics are most important since the pollutants that are emitted in to the atmospheric boundary layer are subjected to gradual dispersion and mixed through the action of turbulence in this region which ultimately facilitate in modelling the vertical extent of the pollutant movement (Parameswaran *et al*., 1997; Menut *et al*., 1999). The maximum in the vertical gradient or the sharp upward decrease in the lidar backscatter return denotes the mixed layer depth, which should be observed as the aerosols content in the mixed layer closer to the ground portion is higher than the air above (Seibert *et al*., 1998). Eddies generated as a result of surface heating are transported vertically up until the rising air parcel encounters a region having equal ambient density. Therefore, the altitude region where eddy transport is significant is referred to as the well-mixed region (Parameswaran, 2001). The altitude profile in Figure 2 shows that the peak value of BSR during monsoon, post-monsoon, winter and pre-monsoon seasons varies from 1000, 600, 1300 and 1450 m, respectively. The same may be considered as representative mixed layer depth for respective seasons. The region above the mixing height shows a sharp decrease in BSR with increasing altitude, which is known as the entrainment region (through which aerosols in the well mixed region intrudes into the upper region). During summer/pre-monsoon season, ventilation coefficient is as high as compared with winter/post-monsoon season (Devara and Raj, 1993). The range corrected photon counts profiles at different timings on an experimental day (13 December 2006) representing the peak of winter over the experimental site are shown in Figure 3. During this period the boundary layer remains very shallow due to low surface temperatures. After the sunset, the surface cools down very fast, consequently the rate of eddy production are abruptly reduced causing quick disappearance of thermal plumes. Therefore the vertical extent of the aerosol layer remains to its minimum level. In Figure 4, night-time variation of the backscatter return observed on 8 October 2006 (upper panel) and 6 March 2007 (lower panel) are shown. The horizontal axis indicates the time of the measurements in IST (IST = UT + 5.5 h) where as the vertical axis denotes the altitude above the ground level (AGL) in kilometres and the magnitude of the backscatter return signal is given as colour scale. The maximum concentration of particles indicates the mixed layer height. Within

DOI: 10.1002/asl

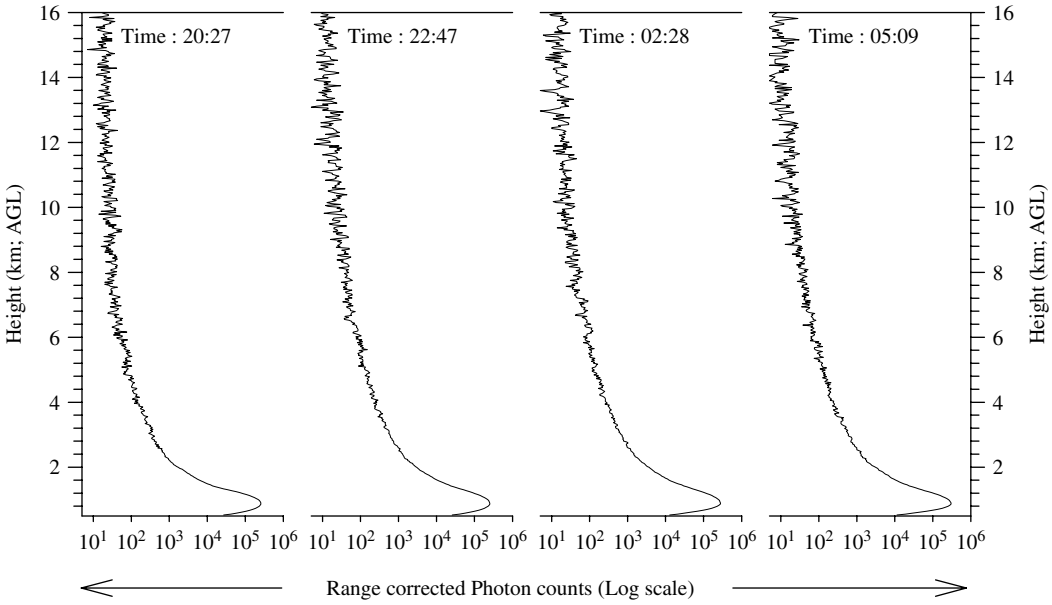

Figure 3. Range corrected photon counts profiles at different timings for 13 December 2006.

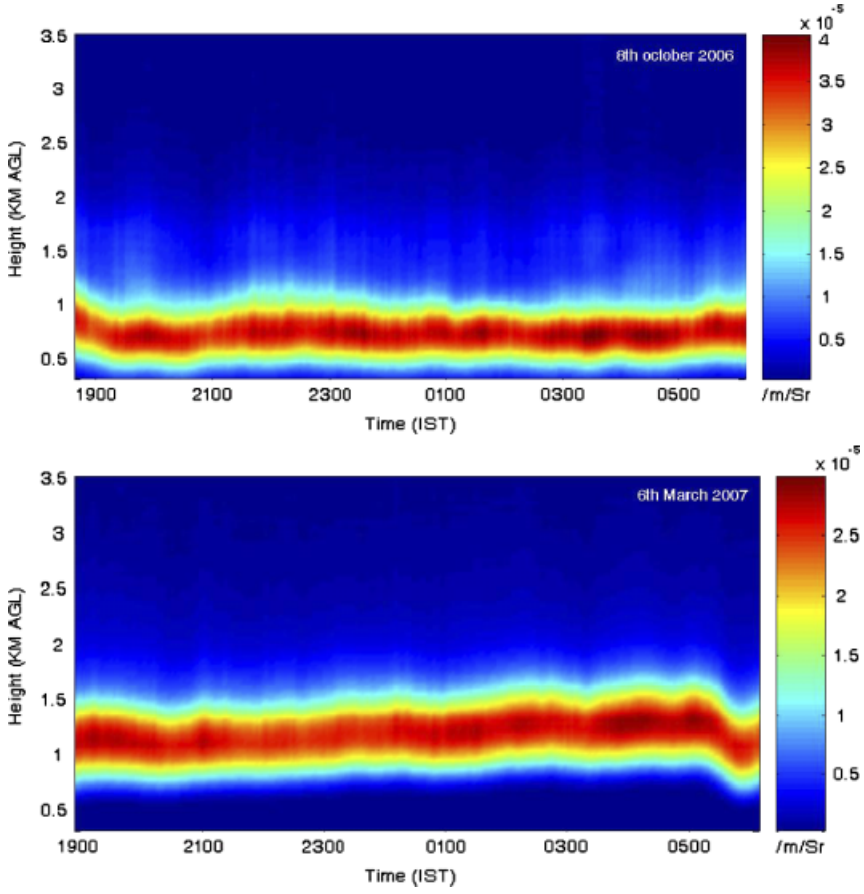

Figure 4. Night-time variation of the attenuated backscatter return, beta (1/m/sr) observed on 8 October 2006 (upper panel) and 6 March 2007 (lower panel).

the mixed layer the thick layer of particles on 8 October 2006 is attributed to the high turbulence. Similarly on the other hand, layers of increased concentration of particles are discernible on 6 March 2007, located at moderately higher altitudes, indicating vertical extent of mixing height. Further, it is quite evident that the different layers of aerosols are clearly distinguished in both the panels, which may be the manifestation of the dust layer of transported origin above the local mixed layer. After sunset the aerosol layers are horizontally stratified because mixing is limited by the surface radiation inversions (Tiwari *et al*., 2003).

DOI: 10.1002/asl

3.4. Aerosol sources

The geographical and climatological features of the observation site mainly determine aerosol characteristics. With the beginning of the summer, over the observing site, the wind direction shifts from southeasterly to southwesterly, consequently the air mass shifts from southern Indian plains (during winter) to the western arid landmass (during summer). The arid landmass includes the Great Indian Thar Desert along the northwestern border of India, which is one of the major sources of atmospheric dust over the Indian subcontinent. As the summer approaches, the northern and northwestern India experiences frequent dust storms due to southwesterly summer winds from the western Thar Desert (Sikka, 1997). In this process the wind, arriving from Thar Desert region, brings the dust particles, which is mainly responsible for the rapid enhancement in the columnar aerosol optical depths (AOD) as observed over the station after March. Meanwhile the higher dust concentration over the region further reinforces the dryness of affected region by suppressing convection (Rosenfeld *et al*., 2001), which has also observed in the present study.

The annual variation in the lidar derived AOD at 532 nm, varied from 0.023 to 0.264 during monsoon and summer seasons, respectively (Table I). Similar trend of temporal variation of AOD values was also observed from Microtops II Sunphotometer (AOD at 500 nm). The higher AOD values during summer 2006 is found, mainly due to the frequent dust storms or entrainment of coarse particles over the observing site as synoptic air mass that flows southwesterly during May and June results in frequent dust loading over northwestern part of India. On the basis of satellite data analysis, Li and Ramanathan (2002) have also shown the eastward transport of west Asian deserts aerosols across the northern Arabian Sea towards the west coast of India. The lower AOD values observed during summer 2007 may be due to the intermittent rains during May 2007. Niranjan *et al*. (2007) have observed the mixing of the anthropogenic aerosol over the Indo-Gangetic plains with the aerosols of desert origin. Satheesh and Srinivasan (2002) have also reported the enhanced values of AOD during summer months over Kashidhoo and Minicoy locations, attributing the transportation of dust particles form arid regions surrounding the Arabian Sea. The minimum AOD observed during winter months may be due to weak-generation mechanisms and lesser possibility of hygroscopic growth of aerosols because of low water vapour content in the atmosphere (Pant *et al*., 2006). During winter months the temperature remains minimum over Indo-Gangetic plains causing a low-level existence of boundary layer height due to capping inversion as well as minimum ventilation coefficient, inhibiting the transport of particles to the free troposphere (Nair *et al*., 2007). Meanwhile, the high value of TOMS aerosol index (AI) found over the study region, indicates the presence of coarse particles in the atmosphere. Further, the monthly mean of AI follows the observed trend in AOD as well as BSR variations over the experimental site. This seasonal cycle in TOMS AI corresponds to the seasonal variability in dust or biomass burning emissions as well as rainfall (Habib *et al*., 2006).

The analysis of back trajectories at 3000 m amsl during the study period indicates when the air mass originates from Arabian region, i.e. the trajectories arriving from the SW direction of the study location (Table I), generally higher values of the backscattering as well as AOD values are observed over the site. While in the rest of the cases, the air parcel could be either from Indian subcontinent or from the Bay of Bengal region.

3.5. Comparison with radiosonde measurements

The vertical variation of temperature, wind direction, wind speed, relative humidity and potential temperature are shown in Figure 5. Owing to non-availability of Radiosonde at observing site, the contemporaneous data on 6 March 2007, were taken from nearest observation station of the Indian Meteorological Department (IMD), Bareilly (28.35 °N and 79.42 °E). These parameters have been used for evaluating the mixing layer heights and to assess the atmospheric boundary layer structure. Figure 5 shows a very well mixed boundary layer up to a height of ∼1200 m, and very strong humidity gradients across the capping inversion at ∼1000 m. The measured vertical variations of potential temperature indicate the atmospheric structure with a well-mixed layer near the surface up to ∼700 m. Above this height the potential temperature increases gradually up to ∼1200 m indicating the stable stratification of aerosols that reduces further vertical mixing. The variation in Planetary Boundary Layer (PBL) structure seems to be in good agreement to those observed lidar and radiosonde profiles. Since the variation in the vertical distributions of aerosol concentration is normally interpreted as aerosol stratification, the variability in the BSR as shown in Figure 4 is most likely caused by temporal variations in the PBL structure, which is also related to the height variation of the above-mentioned meteorological parameters.

3.6. Identification of cirrus clouds

Observations of range corrected photon count profiles have shown the occurrence of cirrus clouds at an altitude ranging from 8 to 10 km AGL. Among the total observations in ∼60% of the cases the occurrence of cirrus clouds were detected. Meanwhile cloud climatology studies based on SAGE II observations have indicated the frequency of cirrus occurrence (AOD ∼0.03), in the tropical and the subtropical regions is up to 70% indicating the radiative effects of cirrus clouds are very large in these regions (Whiteman *et al*., 2004). Photon counts data for three representative days showing the presence of cirrus clouds are shown in Figure 6. The cloud base and top

DOI: 10.1002/asl

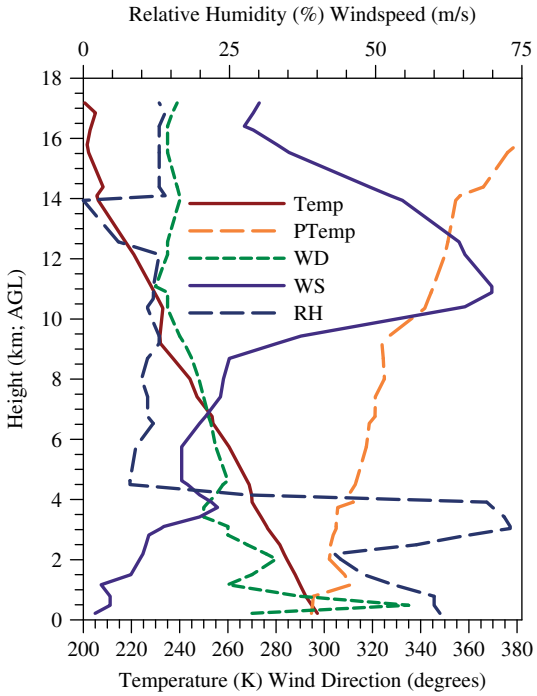

Figure 5. Radiosonde profiles for temperature, potential temperature, wind direction, wind speed and relative humidity measured on 6 March 2007.

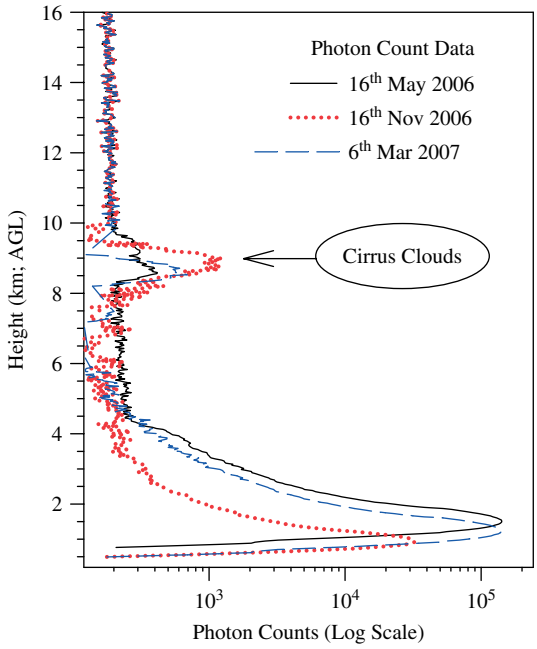

Figure 6. Profiles of photon count data for three representative observation nights showing the existence of cirrus clouds.

heights are found to be 8.2 and 9.1 km, respectively. The corresponding temperatures at these heights are found to be 238 and 242 K, respectively (Figure 5) based on radiosonde measurement on 6 March 2007. The region where these cirrus clouds are observed is found to be highly turbulent (sometimes wind speed up to 68 m/s), indicating that the region of divergence followed by a convergence, showing the favourable conditions for cirrus formation (Parameswaran *et al*., 2003). Over the study region the vertical extent of cirrus was found minimum during winter, indicating that the cirrus clouds observed during the dry period are generally thin in comparison to those observed during the southwest monsoon period (Sunil Kumar *et al*., 2003).

Typical altitude-time contour plot of range corrected photon count on 17 May 2006 is illustrated in Figure 7 showing the presence of cirrus cloud. It is quite discernible from the figure that the cirri is started to be appeared around 2020 (IST) having the base height of ∼8 km AGL, which gradually becomes thick and denser and reaches upto a summit of 9.7 km AGL. The cloud continuously remained strong throughout the observation period. Similarly, the observations on different nights reveal the presence of the cirrus clouds with different structures and patterns with varying vertical extent. Sunil Kumar *et al*. (2003) have reported the observed range for these clouds as 12 to 16 km amsl with a vertical extent ranging from 0.4 to 4 km, on the basis of extended lidar observations at Gadanki (13.5 °N, 79.2 °E). They also calculated that infrared radiative forcing by this tropical cirrus is significantly larger than that due to subtropical cirrus.

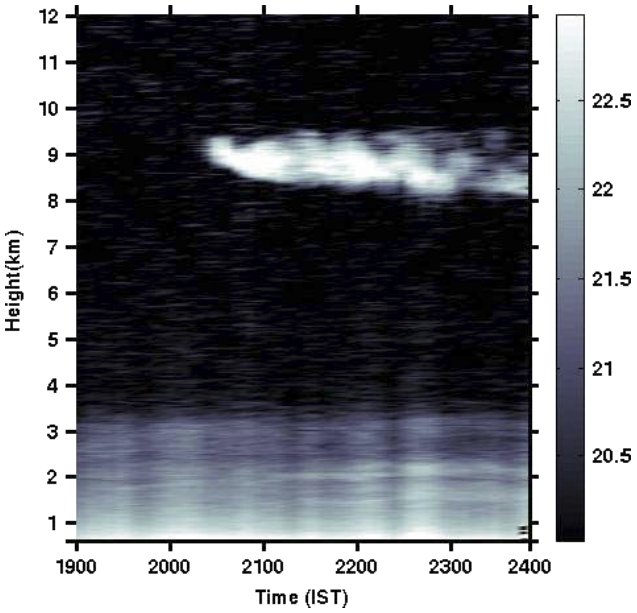

Figure 7. Typical altitude-time contour plots of range corrected photon count on 17 May 2006 showing the presence of cirrus clouds.

4. Conclusions

Lidar observations were carried out for the first time over a high altitude location in central Himalayas. The aerosol backscatter lidar profiles revealed the presence of aerosol layers up to the summit of ∼2 km AGL. The BSR varies from ∼10 to ∼20 with lowest and highest value during post and pre-monsoon, respectively. The seasonal variation in columnar AOD follows the similar trend to those for BSR. Observed values of BSR over study location can represent a free tropospheric background level. The structure of planetary boundary

DOI: 10.1002/asl

layer determined from the lidar data compares reasonably well to those evaluated by using radiosonde data, which suggests that the lidar can be used to characterise the boundary layer structure. The aerosol mixing height fluctuates in the range of 600–1450 m for post-monsoon and pre-monsoon periods respectively; showing a strong dependence on the vertical mixing processes of convective eddies in the atmospheric boundary layer due to varying meteorological condition over the observing site. On several occasions cirrus clouds of varying thickness and duration were successfully detected. The cloud mean altitude was found to be ∼8 to 10 km AGL. Over the study region the vertical extent of cirrus was found minimum during winter as compared to summer.

Acknowledgements

This work was carried out as a part of ABLN&C, under the ISRO–GBP. Authors are thankful to the Directors, ARIES Nainital, and NARL Gadanki for their encouragement to undertake this work. Thanks are due to Arjun Reddy for the help in the lidar observations. Authors are also grateful to anonymous reviewers for their constructive and useful suggestions, which significantly improved the contents of the paper.

References

Bhavani Kumar Y. 2006. Portable lidar system for atmospheric boundary layer measurements. *Journal of Optical Engineering* **45**(7): 076201.

Cambell JR, Welton EJ, Spinhirne JD, Qiang Ji, Tsay Si-Chee, Piketh SJ, Barenbrug M, Holben BN. 2003. Micro pulse lidar observations of tropospheric aerosol over northeastern South Africa during the ARREX and SAFARI 2000 dry season experiments. *Journal of Geophysical Research* **108**(D18): 33-1–33-19.

Charlson RJ, Schwartz SE, Hales JM, Cess RD, Coakley JA Jr., Hansen JE, Hofmann DJ. 1992. Climate forcing by anthropogenic aerosols. *Science* **255**: 423–430.

Cheng AYS, Viseu A, Leong FKC, Chan CS, Tam KS, Chan RLM. 2005. Horizontal Eye-safe Mie Lidar for monitoring of Urban Aerosols in Macao. *Proceedings of SPIE*, Vol. 5984, Singh UN (ed.); Society of Photo-optical Instrumentation Engineers (SPIE): Washington. 59840L–1.

Devara PCS, Ernet Raj E. 1993. Lidar measurements of aerosols in the tropical atmosphere. *Advances in Atmospheric Sciences* **10**: 365–378.

Devara PCS, Raj PE, Sharma S, Pandithurai G. 1995. Real-time monitoring of atmospheric aerosols using a computer controlled lidar. *Atmospheric Environment* **29**: 2205–2215.

Fernald FG. 1984. Analysis of atmospheric lidar observations: Some comments. *Applied Optics* **23**: 652–653.

Habib G, Venkataramana C, Chiapellob I, Ramachandran S, Boucherb O, Shekar Reddy M. 2006. Seasonal and interannual variability in absorbing aerosols over India derived from TOMS: Relationship to regional meteorology and emissions. *Atmospheric Environment* **40**: 1909–1921.

Hegde P, Pant P, Naja M, Dumka UC, Sagar R. 2007. South Asian dust episode in June 2006: Aerosol observations in the central Himalayas. *Geophysical Research Letters* **34**: L23802, DOI:10.1029/2007GL030692.

Immler F, Schrems O. 2002. Determination of tropical cirrus properties by simultaneous LIDAR and radiosonde measurements. *Geophysical Research Letters* **29**(23): 2090, DOI:10.1029/2002GL015076.

IPCC. 2007. Climate Change 2007: The physical science basis, Contribution of Working Group I to the fourth assessment report of the Intergovernmental Panel on Climate Change.

Klett JD. 1985. Lidar inversion with variable backscatter extinction ratios. *Applied Optics* **24**: 1638–1643.

Kovalev VA. 1993. Lidar measurements of the vertical aerosol extinction profiles with range dependent backscatter to extinction ratios. *Applied Optics* **32**: 6053–6065.

Lagrosas N, Yoshii Y, Kuze H, Takeuchi N, Naito S, Sone A, Kan H. 2004. Observation of boundary layer aerosols using a continuously, portable lidar system. *Atmospheric Environment* **38**: 3885–3892.

Li F, Ramanathan V. 2002. Winter to summer monsoon variation of aerosol optical depth over the tropical Indian Ocean. *Journal of Geophysical Research* **107**(D16): 4284. DOI:10.1029/2001JD000949.

Measures RM. 1984. *Laser Remote Sensing, Fundamentals and Applications*. John Wiley and Sons: New York; 510.

Menut L, Flamant C, Pelon J, Flamant PH. 1999. Urban boundary layer height determination from lidar measurements over the Paris area. *Applied Optics* **38**: 945–954.

Mok TM, Rudowicz CZ. 2004. A lidar study of the atmosphere entrainment zone and mixed layer over Hong Kong. *Atmospheric Research* **69**: 147–163.

Murayama T, Masonis SJ, Redemann J, Anderson TL, Schmid B, Livingston JM, Russell PB, Huebert B, Howell SG, McNaughton CS, Clarke A, Abo M, Shimizu A, Sugimoto N, Yabuki M, Kuze H, Fukagawa S, Maxwell-Meier K, Weber RJ, Orsini DA, Blomquist B, Bandy A, Thornton D. 2003. An intercomparison of lidar-derived aerosol optical properties with airborne measurements near Tokyo during ACE-Asia. *Journal of Geophysical Research* **108**(D23): 8651, DOI:10.1029/2002JD003259.

Nair VS, Moorthy KK, Alappattu DP, Kunhikrishnan PK, George S, Nair PR, Babu SS, Abish B, Satheesh SK, Tripathi SN, Niranjan K, Madhavan BL, Srikant V, Dutt CBS, Badarinath K VS, Reddy RR. 2007. Wintertime aerosol characteristics over the Indo-Gangetic Plain (IGP): Impacts of local boundary layer processes and long-range transport. *Journal of Geophysical Research* **112**: D13205, DOI:10.1029/2006JD008099.

Niranjan K, Madhavan BL, Sreekanth V. 2007. Micro pulse lidar observation of high altitude aerosol layers at Visakhapatnam located on the east coast of India. *Geophysical Research Letters* **34**: L03815, DOI:10.1029/2006GL028199.

Nyeki S, Kalberer M, Colbeck I, De Wekker S, Furger M, Gäggeler HW, Kossmann M, Lugauer M, Steyn D, Weingartner D, Wirth M, Baltensperger U. 2000. Convective boundary layer evolution to 4 km asl over high-alpine terrain: Airborne lidar observations in the Alps. *Geophysical Research Letters* **27**(5): 689–692, 10.1029/1999GL010928.

Pant P, Hegde P, Dumka UC, Sagar R, Satheesh SK, Moorthy KK, Saha A, Srivastava MK. 2006. Aerosol characteristics at a high altitude location in central himalayas: Optical properties and radiative forcing. *Journal of Geophysical Research* **111**: D17206, DOI:10.1029/2005JD006768.

Parameswaran K. 2001. Influence of micrometeorological features on coastal boundary layer aerosol characteristics at the tropical station, Trivandrum. *Proceedings of the Indian Academy of Sciences-Earth and Planetary Sciences* **110**: 247–265.

Parameswaran K, Rose KO, Krishna Murthy BV, Osborn MT, Mc Master LR. 1991. Comparison of aerosol extinction profiles from lidar and SAGE-II data at a tropical station. *Journal of Geophysical Research* **96**: 10861–10866.

Parameswaran K, Sunil Kumar SV, Krishna Murthy BV. 2003. Lidar observations of cirrus cloud near the tropical tropopause: temporal variations and association with tropospheric turbulence. *Atmospheric Research* **69**: 29–49.

Parameswaran K, Vijayakumar G, Krishna Murthy BV. 1997. Lidar observations on aerosol mixing height in a tropical coastal environment. *Indian Journal of Radio & Space Physics* **26**: 15–21.

Prasad AK, Singh S, Chauhan SS, Srivastava MK, Singh RP, Singh R. 2007. Aerosol radiative forcing over the Indo-Gangetic plains during major dust storms. *Atmospheric Environment* **41**(29): 6289–6301.

Raj PE, Devara PCS, Pandithurai G, Sharma S. 1996. Cloud-base height estimations by laser radar at Pune. *Indian Journal of Radio & Space Physics* **25**: 74–78.

Rosenfeld D, Rudich Y, Lahav R. 2001. Desert dust suppressing precipitation: A possible desertification feedback loop. *Proceedings of the National Academy of Sciences of the United States of America* **98**(11): 5975–5980.

Satheesh SK, Srinivasan J. 2002. Enhanced aerosol loading over Arabian Sea during the pre-monsoon season: natural or anthropogenic? *Geophysical Research Letters* **29**: 1874.

Seibert P, Kromp-Kolb H, Kasper A, Kalina M, Puxbaum H, Jost DT, SchwiKowski M. 1998. Transport of polluted boundary layer air from the Po Valley to high-alpine sites. *Atmospheric Environment* **32**(23): 3953–3965.

Sikka DR. 1997. Desert climate and its dynamics. *Current Science* **72**(1): 35–46.

Spinhirne JD. 1993. Micro pulse lidar. *IEEE Transaction on Geosciences and Remote Sensing* **31**(1): 48–54.

Stull RB. 1997. *An Introduction to Boundary Layer Meteorology*. Kluwer Academic Publishers: The Netherlands; 666.

Sunil Kumar SV, Parameswaran K, Krishna Murthy BV. 2003. Lidar observations of cirrus cloud near the tropical tropopause: general features. *Atmospheric Research* **66**: 203–227.

Thomas A, Borrmann S, Kiemle C, Cairo F, Volk M, Beuermann J, Lepuchov B, Santacesaria V, Matthey R, Rudakov V, Yushkov V, Mackenzie AR, Stefanutti L. 2002. In situ measurements of background aerosol and subvisible cirrus in the tropical tropopause region. *Journal of Geophysical Research* **107**(D24): 4763, DOI:10.1029/2001JD001385.

Tiwari YK, Devara PCS, Raj PE, Maheskumar RS, Pandithurai G, Dani KK. 2003. Tropical urban aerosol distributions during pre-sunrise and post-sunset as observed with lidar and solar radiometer at Pune. *Indian Journal of Aerosol Science* **34**: 449–458.

Whiteman DN, Demoz B, Wang Z. 2004. Subtropical cirrus cloud extinction to backscatter ratios measured by Raman Lidar during CAMEX-3. *Geophysical Research Letters* **31**: L12105, DOI:10.1029/2004GL020003.